1 DATA PAPER

2 CPT-Based Liquefaction Case Histories Compiled

3 from Three Earthquakes in Canterbury, New

4 Zealand

7

8

9

10

11

12

13

14

15

16

17

18

19

20

- 5 Mertcan Geyin, M.EERI, Brett W. Maurer, M.EERI, Brendon A. Bradley, M.EERI, Brendon A. Bradley,
- 6 M.EERI, Russell A. Green, c) M.EERI, and Sjoerd van Ballegooyd)

Earthquakes occurring over the last decade in the Canterbury region of New Zealand have resulted in liquefaction case-history data of unprecedented quantity. This provides the profession with a unique opportunity to advance the prediction of liquefaction occurrence and consequences. Towards that end, this paper presents a curated dataset containing ~15,000 cone-penetration-test-based liquefaction case histories compiled from three earthquakes in Canterbury. The compiled, post-processed data is presented in a dense array structure, allowing researchers to easily access and analyze a wealth of information pertinent to free-field liquefaction response (i.e., triggering and surface manifestation). Research opportunities using this data include, but are not limited to, the training or testing of new and existing liquefaction-prediction models. The many methods used to obtain and process the case-history data are detailed herein, as is the structure of the compiled digital file. Lastly, recommendations for analyzing the data are outlined, including nuances and limitations that users should carefully consider.

Introduction

- 21 Within the six years following the 4 Sept. 2010 M_w7.1 Darfield earthquake, which triggered
- 22 widespread liquefaction in the city of Christchurch, New Zealand, and its environs, 21 additional

^{a)} University of Washington, Seattle, Washington, United States

b) University of Canterbury, Christchurch, New Zealand

c) Virginia Tech, Blacksburg, Virginia, United States

d) Tonkin + Taylor Ltd., Auckland, New Zealand

23 $M_{\rm w} \ge 5$ earthquakes occurred within ~20 km of the city's center. While some liquefaction was 24 observed in at least 10 of these events (Quigley et al., 2013), damaging liquefaction was most 25 notably triggered by ruptures on 22 Feb 2011, 13 June 2011, 23 Dec 2011, and 14 Feb 2016. A 26 comprehensive summary of the first three of these, including tectonic and geologic settings, 27 seismology, and effects, is provided by Quigley et al. (2016). Specific to liquefaction, observed 28 consequences included: damage to low-, mid-, and high-rise structures, resulting in widespread 29 loss of building stock (e.g., Cubrinovski et al., 2011; van Ballegooy et al., 2014a; Bray et al., 30 2014); failure of water, wastewater, power, and communications networks (e.g., O'Rourke et al., 2014; Kwasinski et al., 2014; Tang et al., 2014); loss of road, rail, bridge, and levee functionality 31 32 (e.g., Green et al. 2011; Wotherspoon et al., 2011; Cubrinovski et al., 2014); and impairment of 33 port infrastructure (e.g., Chalmers et al., 2013). 34 The presence of these effects in a major urban center facilitated and motivated the collection 35 of vast amounts of data, including seismologic, hydrologic, geospatial, and geotechnical 36 measurements, much of which was uploaded to the open access Canterbury Geotechnical Database 37 (CERA, 2013), now the New Zealand Geotechnical Database (NZGD, 2020). These bulk, raw 38 ingredients constitute the makings of an unprecedented quantity of liquefaction case histories, 39 which can be used to train or test predictive models. While several "tiers" of liquefaction prediction 40 model exist (Geyin et al., 2020a), most prevalent models in practice are based on in-situ 41 geotechnical tests, among which the cone-penetration-test (CPT) has important advantages (NRC, 42 2016). Yet, while such models are widely used to predict liquefaction, they have to-date been 43 trained on relatively modest datasets. For example, the CPT-based liquefaction triggering model of Boulanger and Idriss (2014), when developed, was trained on essentially all published case 44 45 histories from all earthquakes combined, or 255 datapoints. Accordingly, this study compiles a 46 curated digital dataset of approximately 14,500 - 15,500 CPT-based case-histories from three 47 earthquakes in Canterbury – namely the Sept. 2010 M_w7.1, Feb. 2011 M_w6.2, and Feb. 2016 M_w5.7

processed data is presented in a structure array (i.e., a single file), allowing researchers to readily access and analyze a wealth of information pertinent to free-field liquefaction response. As shown

earthquakes – with the exact total depending on criteria discussed subsequently. The post-

in Figure 1, this considerably augments the data available for model training and testing (by at

least 50x), presenting the profession with a unique opportunity to advance the science of

53 liquefaction prediction.

48

49

50

51

52

In the following sections, the methods used to obtain, process, and populate the database are first detailed, with each "datapoint" including: (i) identifying information (e.g., geographic coordinates); (ii) processed CPT data, both with and without inverse-filtering and interface correction (Boulanger and DeJong, 2018); (iii) peak ground acceleration (PGA) and earthquake magnitude (M_w); (iv) groundwater table (GWT) depth; and (v) the classified occurrence and severity of liquefaction manifestation at the ground surface, with explicit focus on free-field level ground sites. Next, the structure and formatting of the resulting data array are described, and lastly, recommendations for analyzing the data are discussed, including nuances, uncertainties, and limitations that users should carefully consider.

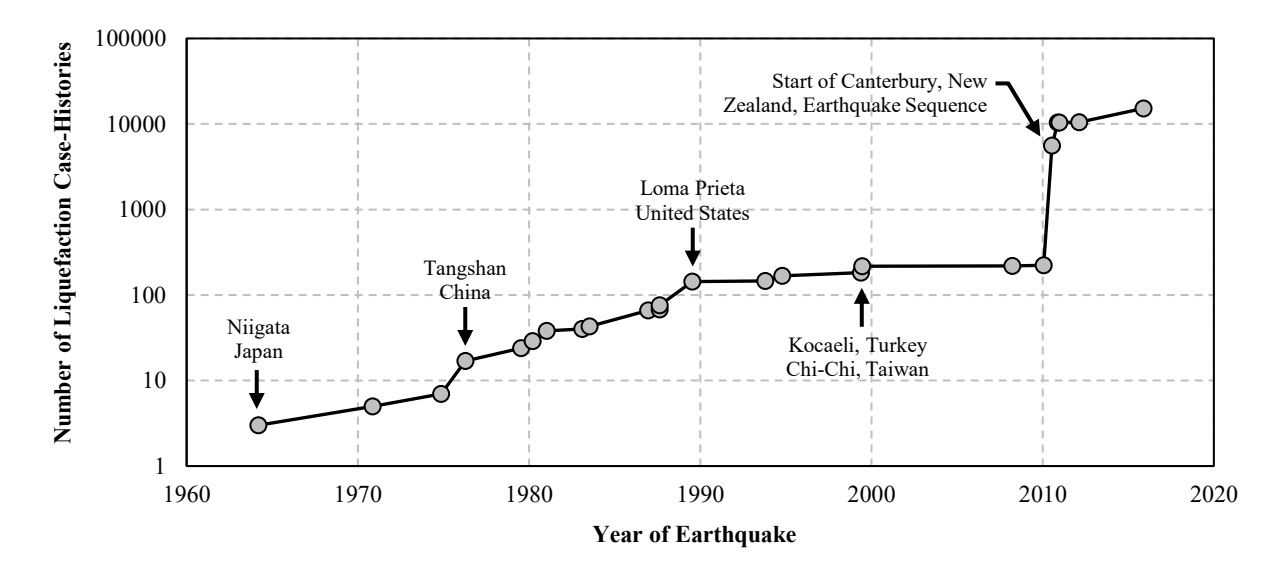


Figure 1. Chronology of CPT-based liquefaction case histories, as compiled by Geyin et al. (2020a).

Methodology

Case histories were compiled from the Sept. 2010 M_w7.1, Feb. 2011 M_w6.2, and Feb. 2016 M_w5.7 earthquakes. This effort built upon successive compilations (Maurer et al., 2014, 2015a), augmenting the largest by more than 50%. While data could potentially also be compiled from the aforementioned events of 13 June and 23 Dec 2011, these events are complicated by the occurrence of multiple, similar-magnitude ruptures only minutes-to-hours apart (Bradley, 2016). As a result, reconnaissance captured the compounded effects of multiple events (complicating observations of response) and pore pressures were elevated at the start of latter events (complicating predictions

- of response). We thus choose not to present these data, focusing instead on three events without
- 72 this obfuscating circumstance.

73

74

75

76

77

78

79

80

81

82

83

84

85

86

87

88

89

90

91

92

93

94

95

96

97

98

99

CPT Data and Processing

CPT data was obtained from the New Zealand Geotechnical Database (NZGD, 2020) at sites where liquefaction manifestations could be reliably classified, as discussed subsequently. During this process, CPTs were rejected if inferred from geospatial autocorrelation analyses (Anselin, 1995) to have terminated prematurely (e.g., due to impedance from gravel), such that liquefiable soils potentially exist at greater depth. The local geology of Christchurch is well characterized, with dense, non-liquefiable soils typically found at a certain depth and unlikely to be underlain by looser soils that contribute to liquefaction hazard. In particular, beach, estuarine, and coastal swamp sediments were deposited across Christchurch as sea level rose during the late Pleistocene and Holocene, reaching a peak ~6,500 years before present, with the coastline located 1-2 km west of the present-day city center (Brown et al., 1995). Since then, alluvial deposition has resulted in progradation of the coast to its present location (Brown et al., 1995). Collectively, the deposits resulting from coastline transgression and progradation are known as the Christchurch formation and overlay Pleistocene gravels (i.e., the Riccarton Gravel formation). The terrestrial thickness of the Christchurch formation is greatest beneath the present-day coastline and tapers from east to west, terminating around the mid-Holocene coastal highstand, beyond which the surface geology is characterized by the Springston formation of alluvial gravels and sands (Begg and Jones, 2012). Thus, where the Springston formation dominates (and in some areas of the Christchurch formation), gravelly soils force CPT termination at shallow depth (< 20 m).

Figure 2 maps the expected, surficial geologic units as described in Table 1, and the locations and termination depths of CPT soundings. The termination-depth trends shown in Figure 2b generally agree with the known geologic profile, such that these depths diminish from east to west. While the possibility of liquefiable soils at greater depths exists, it was assumed for this study that their limits are generally defined by CPT termination depths. However, the database was first parsed using an Anselin Local Morans I analysis (Anselin, 1995) to identify and remove outliers with sounding depths statistically less than the spatial average (i.e., soundings more likely to have prematurely terminated before reaching the Riccarton Gravel formation).

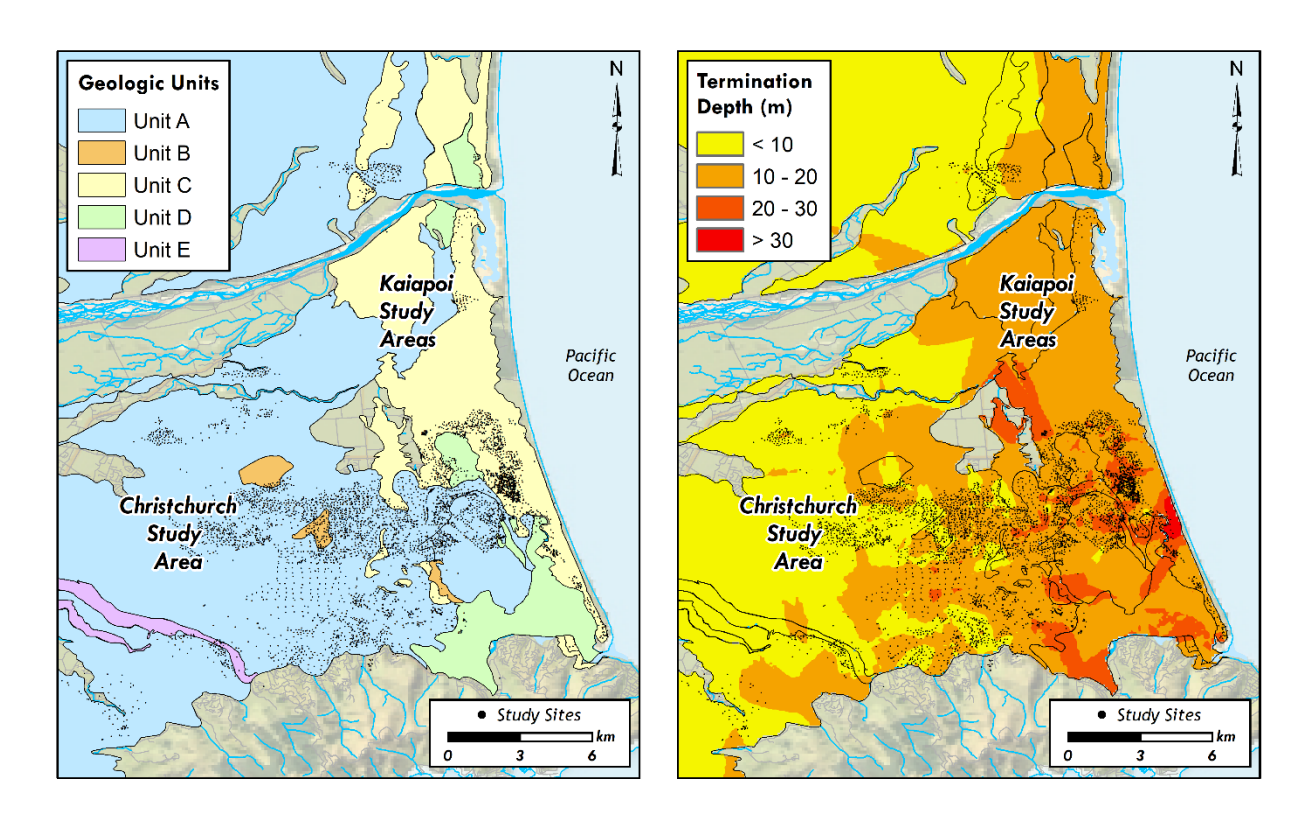


Figure 2. Case-history locations in context of: **(a)** surifical geologic units, as described in Table 1; and **(b)** CPT sounding termination depths, as discussed in the text.

Table 1. Surficial Geologic Units of Study Area.

Geologic Unit	Description	Source	Percent (%) of CPTs in Unit
A	Alluvial sand and silt of overbank deposits	Brown (1975)	59.39
В	Peat swamps now drained	Brown & Weeber (1992)	2.24
C	Fixed dune sand and beach deposits	Brown (1975)	35.34
D	Saline sand, silt and peat of drained lagoons and estuaries Brown & Weeber (1992)		2.26
E	Fluviatile gravel, sand, and silt of historic river flood channels	Brown & Weeber (1992)	0.43

While the CPT offers advantages among in-situ tests used to predict liquefaction, it is still limited by the volume of soil mobilized around the cone. As an intermediate-to-large-strain penetration test, this mobilized zone acts as a physical "low-pass filter" on the true soil

100

101

102

stratigraphy, removing information from the low spatial wavelengths, such as the data defining a thin soil stratum or the interface between two disparate soils. These spatial smoothing effects, which are commonly referred to as "thin layer" and "transition" effects, have long been recognized and studied (e.g., Treadwell 1976; Lunne et al. 1997; Ahmadi and Robertson 2005; Robertson 2011; van der Linden 2018). While chart-based methods exist for manually correcting these effects on CPT data, Boulanger and DeJong (2018) proposed the first programmable procedure. This methodology, referred to as an "inverse filtering and interface detection" procedure, predicts the "true" CPT profile from measured CPT values. Since these measured values reflect a filtered view of reality, their correction would improve subsurface characterization. As a demonstration of the methodology, CPT data from Christchurch is shown in Figure 3, both with and without correction.

103

104

105

106

107

108

109

110

111

112

113

114

115

116

117

118

119

120

121

122

123

124

125

126

127

128

129

130

131

132

133

While the performance of Boulanger and DeJong's (2018) procedure is currently being evaluated (e.g., Yost et al. 2020), its use can change a site's perceived liquefaction hazard, with the direction and magnitude of change dependent on numerous factors. Considering this potential influence, and that the Boulanger and DeJong (2018) procedure might prove to be efficacious, both measured and "true" CPT data are provided in the database. While the reader is referred to Boulanger and DeJong (2018) for complete details, the procedure's "baseline" parameters were used to compute "true" CPT data. This was the case for both the subroutine that inverts tip resistance and sleeve friction, and that which detects and corrects stratigraphic interfaces. These defaults can conceivably be calibrated via site-specific study (e.g., from borings adjacent to a CPT), but the information compiled for this study either was insufficient to attempt calibration or provided insufficient statistical support to justify it. As part of the processing methodology, CPT tip- and sleeve-measurements were aligned using statistical cross-correlation (Buck et al. 2002), both for measured and "true" CPT data. In addition, CPT data was infilled in the "pre-drill" zone (i.e., where borings were used to safety bypass pavements or utilities, most often to a depth of ~1 m where applicable (~40% of CPTs were pre-drilled)). In the absence of this correction, the recorded data is that of noise as the cone penetrates an open boring. Accordingly, CPT data was sampled 15 cm beyond the recorded depth of pre-drill, then uniformly applied to the pre-drill interval. While this provides reasonable data for approximating soil unit weights, and by corollary, in-situ stresses below the pre-drill zone, users should consider the relative depths of pre-drill and groundwater when analyzing case histories, as further discussed herein. As part of this process, CPTs with unknown pre-drill depth were preemptively removed from the dataset, as were CPTs

with pre-drill depth exceeding 2.5 m. All CPT processing was completed using the software *Horizon* (Geyin and Maurer, 2020a), a freely-available program developed by the authors.

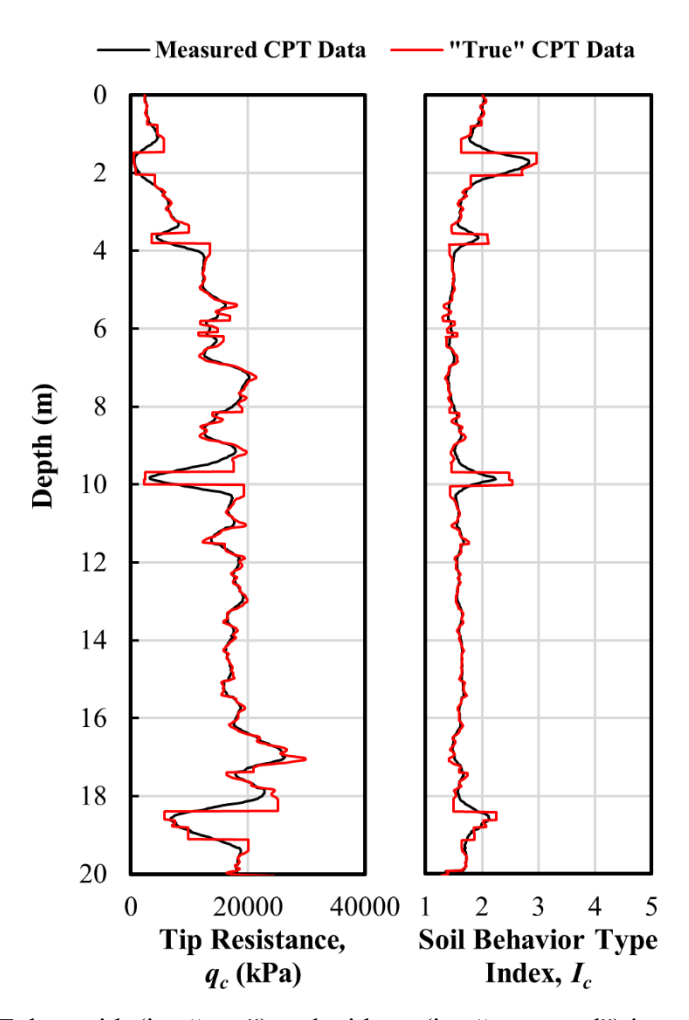


Figure 3. Example CPT data with (i.e. "true") and without (i.e. "measured") inverse-filtering and interface correction via the Boulanger and DeJong (2018) procedure, as implemented in the software *Horizon* (Geyin and Maurer, 2020a).

Liquefaction Manifestations

Emphasis was placed on compiling case histories from free field level-ground sites, with the occurrence and severity of surface manifestation defined primarily by liquefaction ejecta. In this respect, sites with other indicators of liquefaction (e.g., evidence from ground-motions or foundation settlements) were expressly omitted. While \sim 7% of case histories were characterized by a predominance of lateral spreading, the majority were compiled from level-ground sites. In particular, surface manifestations were observed at CPT sites following at least one of the three

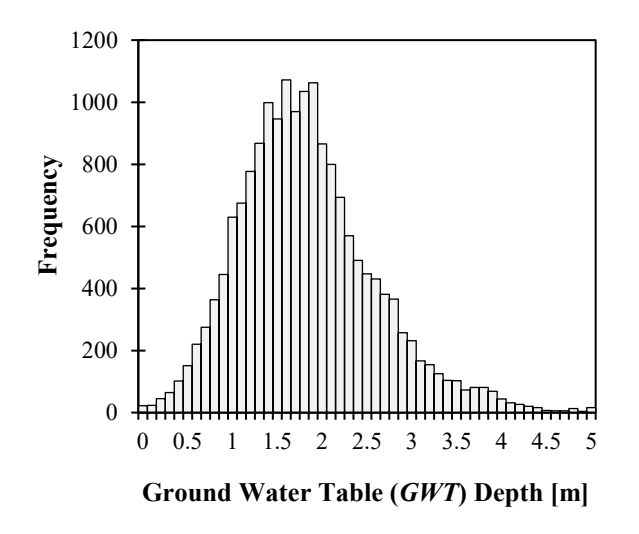
aforementioned earthquakes and manually classified by the authors as "none," "marginal," "moderate," "severe," "lateral spreading," or "severe lateral spreading" using criteria modified from Green et al. (2014) and given in Table 2; the identifying codes assigned herein to each classification are also provided. This was accomplished using high-resolution satellite imagery and reconnaissance reports available in the New Zealand Geotechnical Database (NZGD, 2020). Classifications were based on a circular sample area, centered on each CPT, with approximate radius of 10 m. Representative observations of manifestation classifications are provided in Appendix A. Sites where surface manifestations could not be reliably classified following an event are denoted as "unknown" and coded "10" (i.e., sites where manifestations were classified following at least one earthquake, but not all three, which was the case for ~18% of study sites). Of the resulting 15,890 compiled case histories, 61% were classified as "none" and 39% are cases in which manifestations were observed and classified in accordance with Table 2. Owing to nuances that will be discussed subsequently, the quantity of data best suited for model training and testing is ultimately reduced to ~14,500 – 15,500 cases.

Table 2. Criteria used to classify liquefaction manifestations (after Green et al. 2014).

Classification	Severity ID	Criteria	
None	0	No observed liquefaction ejecta or lateral spreading	
Minor	1	Small, isolated liquefaction features less than a vehicle width; <5% of ground surface is covered by ejecta; no lateral spreading.	
Moderate	2	Groups of liquefaction features greater than a vehicle width; 5-40% of ground surface is covered by ejecta; streets are generally passable; no lateral spreading.	
Severe	3	Adjoining large liquefaction features that are greater than a vehicle width >40% of ground surface is covered by ejecta; streets are generally impassable; no lateral spreading.	
Lateral Spreading	4	Ejection of liquefied material at the ground surface may be observed, but lateral spreading is the predominant manifestation and damage mechanism. Measured crack-displacement widths are less than 200 mm.	
Severe Lateral Spreading	5	Ejection of liquefied material at the ground surface may be observed, but lateral spreading is the predominant manifestation and damage mechanism. Measured crack-displacement widths exceed 200 mm.	
Unknown	10	Insufficient information to reliably classify: out of bounds, no reliable documentation, obscured or otherwise ambiguous imagery.	

Hydrologic Data

GWT depths at CPT locations were obtained from the time-dependent models of van Ballegooy et al. (2014b). These models, which reflect seasonal and local fluctuations across the region, were derived in part using long-term monitoring data from a network of ~1000 monitoring wells and provide a best estimate of GWT depths at the time of each earthquake. Well measurements were corrected for elevation changes caused by the earthquakes using digital elevation models derived from ground-based surveys and airborne LiDAR (Light Detection and Ranging). River and coastline data were used to shape and position GWT contours at places of significant groundwater-surface water interaction (van Ballegooy et al., 2014b). The median GWT diminishes from 10+m elevation (relative to sea level) west of Christchurch to less than 1 m elevation in the eastern suburbs (i.e., near the coast), roughly consistent with the change in ground elevation. The GWT depth is generally 1-2.5 m beneath much of the study area but reaches 5 m west of the city center. A histogram of GWT depth for all compiled case histories is shown in Figure 4a.



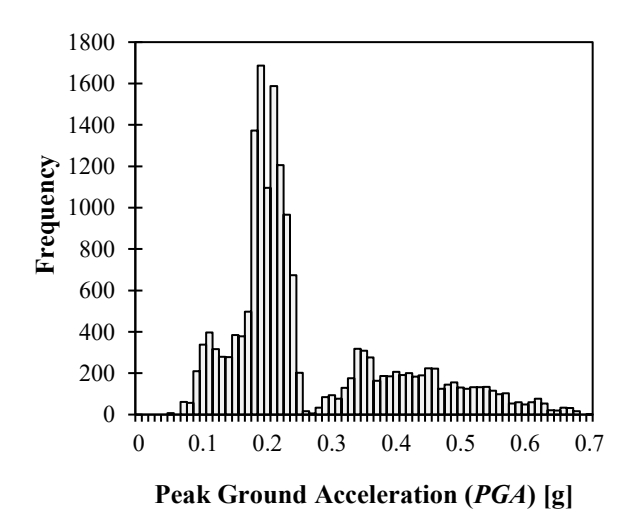


Figure 4. Histograms of: (a) ground water table (GWT) depth; and (b) peak ground acceleration (PGA) for case histories compiled in the curated dataset.

Peak Ground Accelerations (PGAs)

PGA is to-date the most common ground-motion intensity measure (IM) for quantifying seismic demand in liquefaction models. Among other standard IMs, it has been shown to be the most efficient predictor of pore-pressure generation and the initiation of liquefaction (Sideras, 2019). In this study, *PGAs* were estimated at CPT sites via the Bradley (2014) method, which has been used

widely in research related to the Canterbury earthquakes (e.g., van Ballegooy et al. 2015; Geyin et al. 2020a; Geyin and Maurer 2020b). This method geostatistically coalesces instrumentally recorded *PGA*s with predictions from ground-motion models (GMMs), where the former were recorded by more than 20 near-source strong-motion stations (SMS) (e.g., Bradley and Cubrinovski, 2011; Bradley, 2012). Using this approach, the *PGA* at SMS, *i*, is expressed as:

$$\ln (PGA_i) = \mu_{\ln PGA_i}(\text{Site}, \text{Rup}) + \eta + \varepsilon_i, \tag{1}$$

where $\ln(PGA_i)$ is the natural logarithm of the observed PGA at SMS i; $\mu_{\ln PGA_i}$ (Site, Rup) is the mean of the natural logarithm of PGA at SMS i predicted by a GMM, which is a function of site and rupture parameters; η is the inter-event residual; and ε_i is the intra-event residual. Within Equation 1, a GMM predicts a PGA distribution:

$$ln(PGA_i) \sim N(\mu_{lnPGA_i}, \sigma_{\eta}^2 + \sigma_{\varepsilon}^2), \qquad (2)$$

where $X \sim N(\mu_X, \sigma_X^2)$ is shorthand notation for X having a normal distribution with mean, μ_X , and variance, σ_X^2 . By definition, all PGAs recorded in a given earthquake have the same inter-event residual, η . Conversely, the intra-event residual, ε_i , varies from site to site but is correlated spatially due to similarities in path and site effects. Accordingly, PGAs at SMS locations can be used to compute conditional distributions of PGAs at CPT locations. First, the Bradley (2013) New Zealand GMM was used to compute the unconditional distribution of PGAs at SMS locations. A mixed-effects regression was then used to determine the inter-event residual, η , and the intra-event residuals, ε_i 's, for each strong-motion station (e.g., Abrahamson and Youngs 1992; Pinheiro et al. 2008). Second, the covariance matrix of intra-event residuals was computed by accounting for the spatial correlation between SMS locations and a test site of interest. The joint distribution of intra-event residuals at a site of interest and the SMS is given as:

$$\begin{bmatrix} \varepsilon^{site} \\ \varepsilon^{SMstation} \end{bmatrix} = N \begin{pmatrix} \begin{bmatrix} 0 \\ \mathbf{0} \end{bmatrix}, \begin{bmatrix} \sigma_{\varepsilon^{site}}^2 & \Sigma_{12} \\ \Sigma_{21} & \Sigma_{22} \end{bmatrix} \end{pmatrix}, \tag{3}$$

where $X \sim N(\mu_X, \Sigma)$ is shorthand notation for X having a multivariate normal distribution with mean μ_X and covariance matrix Σ (i.e., same as above, but in vector form, with bold denoting vectors or matrices); and $\sigma_{\varepsilon^{site}}^2$ is the variance of the intra-event residual at the site of interest. In Equation 3, the covariance matrix has been expressed in a partitioned fashion to elucidate the

subsequent computation of the conditional distribution of ε^{site} . The individual elements of the covariance matrix were computed from:

$$\Sigma(i,j) = \rho_{i,j} \, \sigma_{\varepsilon i} \sigma_{\varepsilon j} \tag{4}$$

where $\rho_{i,j}$ is the spatial correlation of intra-event residuals between two locations i and j, and $\sigma_{\varepsilon i}$ and $\sigma_{\varepsilon j}$ are the standard deviations of the intra-event residual at locations i and j. Based on the joint distribution of intra-event residuals given by Equation 3, the conditional distribution of $\varepsilon^{\text{site}}$ was computed from Johnson and Wichern (2007):

210
$$\left[\varepsilon^{site} \middle| \varepsilon^{SMstation}\right] = N(\Sigma_{12} \cdot \Sigma_{22}^{-1} \cdot \varepsilon^{SMstation}, \sigma_{\varepsilon^{site}}^2 - \Sigma_{12} \cdot \Sigma_{22}^{-1} \cdot \Sigma_{21})$$
209
$$= N(\mu_{\varepsilon^{site}} \middle|_{\varepsilon^{SMstation}}, \sigma_{\varepsilon^{site}}^2 \middle|_{\varepsilon^{SMstation}})$$
(5)

Using the conditional distribution of the intra-event residual given by Equation 5 and substituting into Equation 2, the conditional distribution of PGA at a site of interest, PGA_{site} , is:

$$[ln PGA_{site} | ln PGA_{SMstation}] = N(\mu_{lnPGA_i} + \eta + \mu_{\varepsilon^{Site}|_{\varepsilon^{SMstation}}} \sigma_{\varepsilon^{Site}|_{\varepsilon^{SMstation}}}^2)$$
 (6)

That is, the conditional distribution of PGA is a lognormal random variable completely defined by the conditional median and conditional uncertainty (i.e., lognormal standard deviation). Intuitively, in cases where a CPT is located far from any SMS, the conditional distribution (i.e., final estimate of PGA) is similar to the unconditional distribution (i.e., GMM estimate of PGA), and for a CPT very near to a SMS, the conditional distribution approaches the value observed at the SMS. The conditional median and conditional uncertainty of PGA, both of which are given in the dataset, were computed at CPT sites using the spatial correlation model of Goda and Hong (2008). A histogram of the median PGA values for all case histories is shown in Figure 4b.

One benefit of the adopted approach is that uncertainty is explicitly computed, rather than subjectively assigned, which prior compilations and studies of liquefaction case-history data have been resigned to. With respect to the computed values, GMMs generally have standard deviations of ~ 0.45 -0.55 in the natural log of PGA, though it can be larger in some cases (e.g., Bradley 2013). In the compiled database, this parameter varies from 0.045 to 0.55, with a median of ~ 0.33 . Thus, the PGA uncertainty is generally much less than that which would be obtained using a GMM alone. Any percentile, x, of the conditional PGA distribution may be computed as:

$$PGA_x = PGA_{50} * \exp(n\sigma_{lnPGA})$$
 (7)

where PGA_x is the value of PGA for the x^{th} percentile, PGA_{50} is the conditional median, σ_{lnPGA} is the conditional lognormal standard deviation, and n is the "z-value" of the standard normal distribution for the x^{th} percentile, which is the number of standard deviations from the median. As an example, the 16^{th} and 84^{th} percentiles of a PGA distribution are computed using n values of -1 and 1, respectively, and the PGA_{50} and σ_{lnPGA} values computed for each case history. Maps of these values are available in the New Zealand Geotechnical Database (NZGD, 2020). Additional information describing the preceding methodology is provided by Bradley and Hughes (2012).

Data Structure

The compiled post-processed data is presented in a structure array (i.e., a single file), with each case history including: identifying information (e.g., ID, geographic coordinates); CPT data, both with and without inverse-filtering and interface correction; earthquake magnitude (M_w) ; the median and uncertainty (i.e., lognormal standard deviation) of the conditional PGA; GWT depth; and the classified occurrence and severity of surficial liquefaction manifestation.

The curated dataset is available via the NHERI DesignSafe Cyber-Infrastructure data depot at Geyin et al. (2020b) (https://doi.org/10.17603/ds2-tygh-ht91) and provided in both Matlab data format and as a python data frame. The data fields, classes, contents, and their units are described in Table 3 and its accompanying footnotes. The structure of the data array is depicted in Figure 5 and arranged such that case histories are principally sorted by a CPT identification (ID) number, wherein multiple liquefaction case histories may be accessed. Event-specific data fields (e.g., M_w and PGA) are 3 x 1 arrays containing information from the 2010, 2011, and 2016 earthquakes, respectively. CPT measurements, which are depth-dependent but not event-specific, are l_i x 1 arrays, where l_i is the length of CPT i. Other fields include CPT ID, geographic coordinates, predrill depth, and test date. To provide users with a benchmark against which data re-use scripts may be verified, all relevant data is provided for one case-history site in Appendix B. Recommendations for analyzing these data are next discussed, including important nuances and limitations that users should consider prior to analysis.

Table 3. Data fields, typologies, descriptions, and units.

Field	Class	Content
ID	cell	¹ CPT identifier assigned in the field (non-unique)
CPTname	char	CPT name assigned by the current authors (unique)
FILEname	char	File name from which CPT data was obtained (unique)
Date	datetime	Date CPT conducted
NorthingNZMG	double	NZMG – y coordinate
EastingNZMG	double	NZMG – x coordinate
NorthingWGS84	double	WGS – y coordinate
Easting WGS84	double	WGS – x coordinate
depth	double	Depth below the ground surface [m]
qc	double	Measured tip resistance [kPa]
qc_inv	double	² True tip resistance [kPa]
fs	double	Measured sleeve friction resistance [kPa]
fs_inv	double	² True sleeve friction resistance [kPa]
u2	double	CPT pore pressure measurement, if present [kPa]
pd	double	Pre-drill depth [m]
Magnitude	struct	³ Earthquake moment magnitude (M _w)
PGA	struct	³ Event-specific conditional median peak ground acceleration [g]
PGAsigma	struct	³ Event-specific conditional lognormal standard deviation of PGA
GWT	struct	³ Event-specific groundwater table depth [m]
Manifestation	struct	^{3,4} Classified type/severity of surface manifestation

¹CPT IDs from original CPT data (.csv or .xlsx files), which were recorded by field engineers and are non-unique in the dataset.

²Processed per the Boulanger and DeJong (2018) procedure; specifically, using the "baseline" inversion model.

 $^{^3}$ There are three earthquakes within the fields from which event-specific data is compiled: $M_w7.1~4$ Sept 2010 (Yr2010), $M_w6.2~22$ Feb 2011 (Yr2011), and $M_w5.7~14$ Feb 2016 (Yr2016).

⁴The occurrence/severity of surface manifestation was manually classified for each CPT location in each earthquake per the criteria in Table 2. Classifications are based on a circular sample area, centered on each CPT, with approximate radius of 10 m.

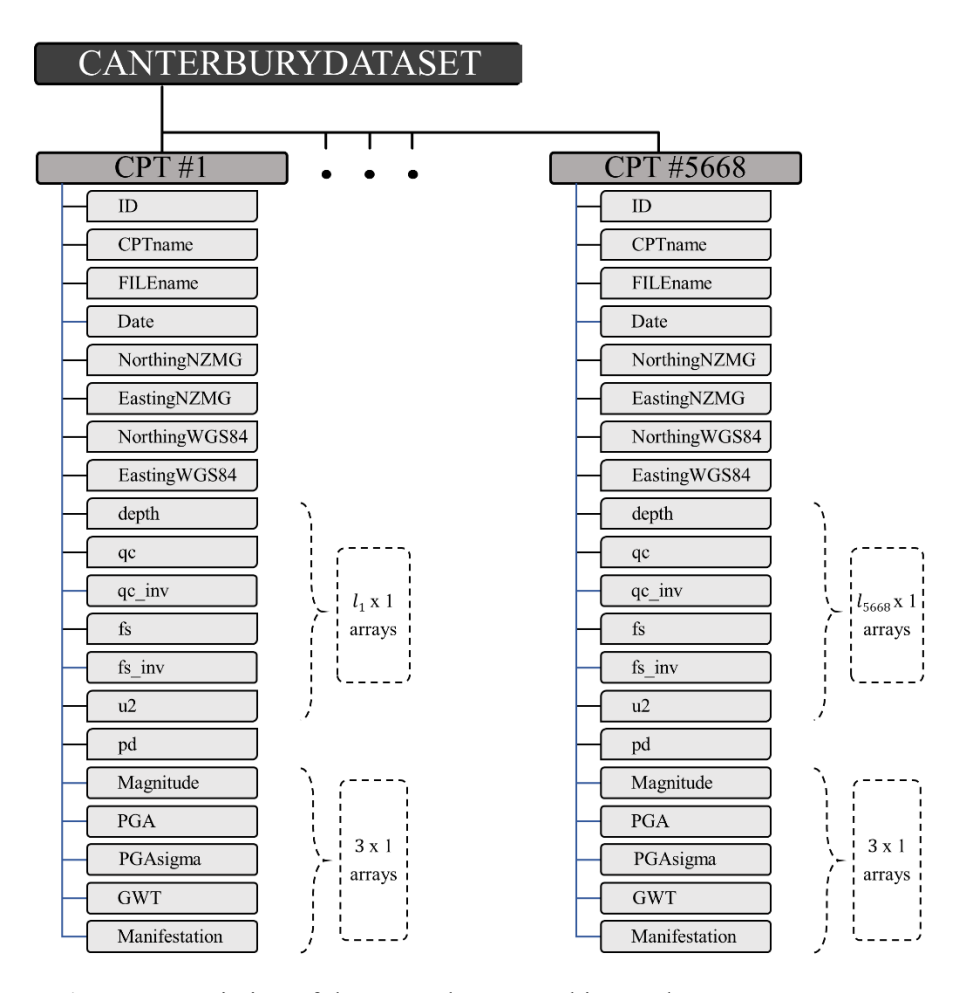


Figure 5. Depiction of the Canterbury case-history dataset structure array.

Discussion: Data Nuances, Alternatives, and Analysis

The compiled, post-processed data allows researchers to easily access and analyze a wealth of information pertinent to in-situ site characterization and free-field liquefaction response (i.e., triggering and surface manifestation). Research opportunities using this data include, but are not limited to: (i) methods for quantifying/simulating subsurface spatial variability; (ii) training or testing of new and existing liquefaction-prediction models; (iii) temporal assessment of CPT data during shaking sequences, including use of aging-correction factors for liquefaction prediction (i.e., K_{DR}); and (iv) evaluation of CPT inversion filters in the context of liquefaction model performance. Prior to such analyses, however, users should carefully consider several important data nuances, alternatives, and limitations. These topics are discussed as follows and ordered by: (i) additional data exclusion criteria; (ii) alternative sources of data; (iii) correlations and decisions for analysis; and (iv) lingering uncertainties.

Additional Data Exclusion Criteria

GWT and CPT Pre-drill Depths. As discussed previously, CPTs in which the pre-drill depth exceeded 2.5 m were preemptively removed from the dataset. For the remainder of CPTs, the pre-drill interval (typically \sim 1 m when present) was infilled with CPT data from just below the pre-drill (i.e., where the sensors began penetrating undisturbed soil). While this provides reasonable data for estimating in-situ stresses, users performing liquefaction studies should consider the relative depths of pre-drill and groundwater. Case histories in which the depth of pre-drill exceeds that of the groundwater have additional uncertainty, given that CPT data below the expected water table is extrapolated, rather than measured. A histogram of the GWT depth minus pre-drill depth is shown in Figure 6 for the 15,890 compiled case histories. Of these, 1,503 have pre-drill depth exceeding the GWT depth. However, this differential exceeds 0.5 m for just 420 cases, and exceeds 1 m for just 52 cases. Nonetheless, analysts might exclude some or all such cases to avoid near-surface site-characterization uncertainty. Some 1D liquefaction manifestation models, for example, are especially sensitive to this uncertainty owing to depth-weighting functions (e.g., Ballegooy et al., 2014a; Maurer et al., 2015b).

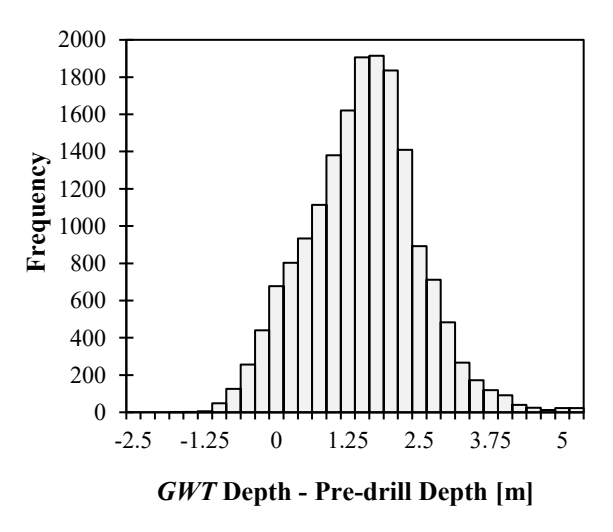


Figure 6. Histogram of ground water table (GWT) depth minus pre-drill depth, for compiled case histories.

PGAs. Profiles subjected to a *PGA* less than the expected threshold for inducing pore pressure (Dobry et al. 1982) might not provide meaningful data for testing liquefaction analytics. That is, if the expected peak strain is less than the volumetric threshold shear-strain for a very loose soil, the absence of liquefaction is easily predicted by judgment. Using such cases to test liquefaction

models could thus increase the prediction efficiency in a misleading manner. Accordingly, analysts might select a site-specific PGA threshold for excluding data, or a general threshold considering the most susceptible soil that could be encountered (e.g., de Magistris et al., 2013). Considering all compiled cases, 0.096 g was the lowest PGA for which surface manifestation of liquefaction was observed, albeit this is distinctly different from that which may induce pore pressure at depth. Of the 15,890 compiled case histories, 98 have PGA less than 0.075 g (see Figure 4b).

Model Applicability. Lateral spreading is a distinct manifestation of liquefaction influenced by topographic factors that were not compiled in this study, but which could be sampled (e.g., ground slope, distance to free face). However, users should consider whether such case histories are appropriate for model training or testing. As an example, 1D liquefaction manifestation models may not fully account for the factors known to cause lateral spreading and can thus predict it poorly (e.g., Maurer et al. 2015c; Rashidian and Gillins 2018). Accordingly, for some purposes, it may be most appropriate to exclude such cases from analysis. Of the 15,890 compiled case histories, 1,110 are cases in which lateral spreading was the predominant manifestation of liquefaction. For further coverage of lateral spreading in Canterbury, see Cubrinovski and Robinson (2016).

Alternative Sources of Data

Ground Motions. As previously outlined, PGAs were obtained by statistically coalescing strongmotion records with GMM predictions (Bradley 2014), the general concept of which is common, and which could be used to obtain other IMs of interest. Notably, liquefaction likely occurred at some SMS sites during the Canterbury earthquakes, potentially effecting measured PGAs and inturn the adopted approach. In particular, evidence of liquefaction was observed in several SMS records from the 22 Feb 2011 earthquake (e.g., Bradley and Cubrinovski 2011), namely: (i) high-frequency acceleration spikes, inferred to result from cyclic mobility/dilation response (Kramer et al. 2016); and (ii) subsequent reduction in high-frequency motion, inferred to result from the softening of liquefaction (Kramer et al. 2016). One such example is shown in Figure 7. It can be seen that a recorded PGA, if associated with a high-frequency dilation spike, could exceed the peak acceleration prior to liquefaction, and possibly, that which would have occurred in its absence (i.e., from the time of liquefaction onward). Wotherspoon et al. (2015) identified four such SMS records (station codes CBGS, CCCC, NNBS, and REHS) and proposed reducing PGAs to those observed prior to interpreted dilation spikes. Adopting these values within a liquefaction analysis,

Upadhyaya et al. (2019) suggested that existing prediction models performed slightly better using the corrected values. However, given that liquefaction obscures SMS records following its onset, the "true" PGAs cannot be known. Whereas dilation spikes may inflate the PGA, selecting a peak value prior to any evidence of liquefaction may artificially depress it. Nonetheless, users should be aware of this issue.

Regardless of which *PGA*s are used within the adopted Bradley (2014) approach, they could be less accurate when complex local phenomena are not captured by empirical predictions (e.g., the effects of rupture directivity, basin-generated surface waves, and near-surface stratigraphic and topographic features). In contrast, physics-based simulations can provide insight into these phenomena via explicit modeling of kinematic fault rupture, wave propagation, and the subsurface velocity structure, thereby predicting IM patterns more accurately. Users may thus be interested in the physics-based simulations of Bradley et al. (2017), which predict both common IMs and full acceleration time-series for each of the three earthquakes in the dataset. These may be obtained at case-history coordinates via the SeisFinder (2020) web portal.

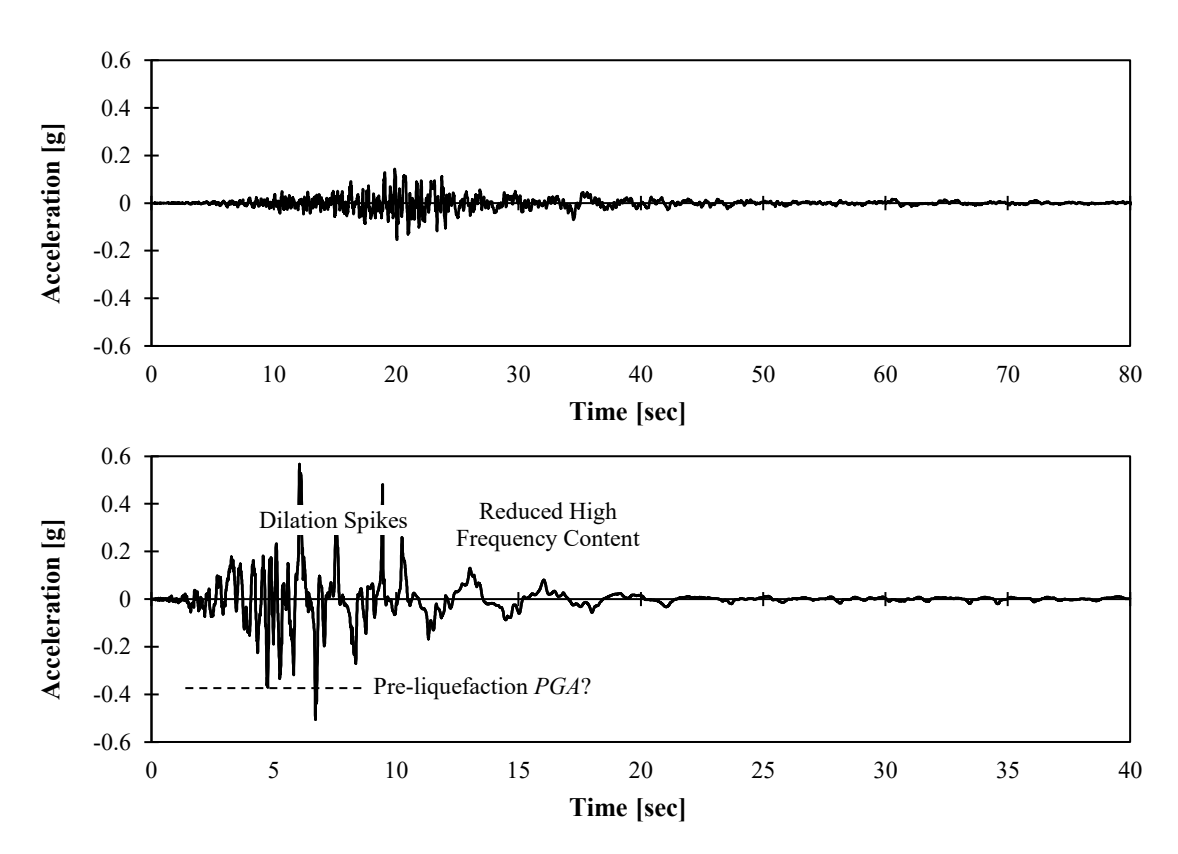


Figure 7. Ground-motion records (SMS code NNBS) during the: **(a)** M_w 7.1 Sept 2010 Darfield; and **(b)** M_w 6.2 Feb 2011 Christchurch earthquakes, showing the effects of liquefaction on recorded PGAs.

Liquefaction Manifestations. As previously discussed, surface manifestations were manually classified at individual CPT sites using a circular sample with 15 m radius. Inherent to this process, which required hundreds-to-thousands of hours to complete, sites where manifestations could not be reliably classified are denoted "unknown." These sites either lacked ground reconnaissance data, were beyond the bounds of high-resolution satellite imagery, had obscured or otherwise ambiguous imagery, or lacked sufficient and consistent information to support classification. Following a similar approach, but without concern for CPT locations or compiling case histories, Townsend et al. (2016) presented maps for the Sept 2010 and Feb 2011 earthquakes wherein observed manifestations are enclosed by polygons and assigned a confidence rating of "certain," "probable," "possible," or "uncertain." These polygons could supplement/replace the classifications made herein or could provide additional quality control. While Townsend et al. (2016) provide a high-quality dataset, caveats for use include: (i) polygons and ratings are for positive observations only (i.e., they do not explicitly delineate negative observations or assign the confidence therein, although a lack of liquefaction may be inferred where polygons are not present); (ii) the mapping does not classify the severity of liquefaction, which may be useful for model training/testing; and (iii) due to the scale of polygons (e.g., that of building parcels), a polygon may be classified as positive but lack manifestations over some or much of its surface area. For these reasons, the classifications made herein may differ from those of Townsend et al. (2016). Nonetheless, users should be aware of this excellent database and consider its use.

Correlations and Decisions for Analysis

331

332

333

334

335

336

337

338

339

340

341

342

343

344

345

346

347

348

349

350

351

352

353

354

355

356

357

358

359

Liquefaction Susceptibility. Existing "simplified stress-based" triggering models (e.g., Robertson and Wride 1998; Moss et el. 2006; Boulanger and Idriss 2014; Green et al. 2019) are not intended to be applied to high plasticity, fine grained, "non-liquefiable" soils, which could result in less accurate predictions of cyclic response, and for which other, more appropriate methods exist (e.g., Boulanger and Idriss 2007). Soils not susceptible to liquefaction triggering are thus generally identified and screened from analysis, consistent with the development of the models. Various criteria based on lab indices have been proposed for this purpose (e.g., Polito 2001; Seed et al. 2003; Bray and Sancio 2006; Boulanger and Idriss 2006), an overview of which is given by Green and Ziotopoulou (2015). However, while soil samples may be obtained using a CPT push-sampler,

continuous sampling and testing to assess susceptibility is prohibitively expensive. For this reason, the CPT soil-behavior-type index (I_c) proposed by Jeffries and Davies (1993) and modified by Robertson and Wride (1998) is generally used to assess susceptibility by way of correlations with lab criteria. For example, an $I_c = 2.6$ threshold is common, such that soils with $I_c < 2.6$ are inferred to be liquefiable (Robertson and Wride 1998). However, because I_c boundaries between soil types are approximate, regional refinement may be needed for optimal efficiency (e.g., Pease 2010; Li et al. 2007). Accordingly, analysts of the data compiled herein may be interested in the susceptibility correlations of Maurer et al. (2019), developed specifically for soils in Christchurch. Using these correlations, the probability that a soil is "susceptible" to liquefaction is:

$$P_{susceptible}(I_c) = 1 - \Phi\left[\frac{\ln(I_c/x_m)}{\beta}\right]$$
 (8)

where Φ is the Gaussian cumulative distribution function; x_m is the median value of the distribution (the value of I_c corresponding to 50% probability); and β is the logarithmic standard deviation. Using this form, Maurer et al. (2019) correlated I_c to four criteria based on Atterberg limits, the coefficients for which are provided in Table 4, and an example of which is shown in Figure 8. Here, "susceptible" generically refers to the varying definitions adopted by the respective works. For example, the Boulanger and Idriss (2006) criterion was explicitly developed to determine the most appropriate analysis procedure for predicting cyclic response, based on whether the soil's expected behavior is "sand-like" or "clay-like." For deterministic analyses in which a single I_c threshold is desired, the median value of the probability distribution (x_m) is recommended, such that soils with I_c exceeding x_m are not susceptible per the underlying criterion.

Table 4. Model coefficients for I_c -susceptibility relationship (Equation 8) (Maurer et al. 2019).

Susceptibility Criterion	β	χ_m
Boulanger and Idriss (2006)	0.0851	2.5031
Polito (2001)	0.0988	2.5474
Seed et al. (2003)	0.1348	2.6214
Bray and Sancio (2006)	0.1275	2.7315

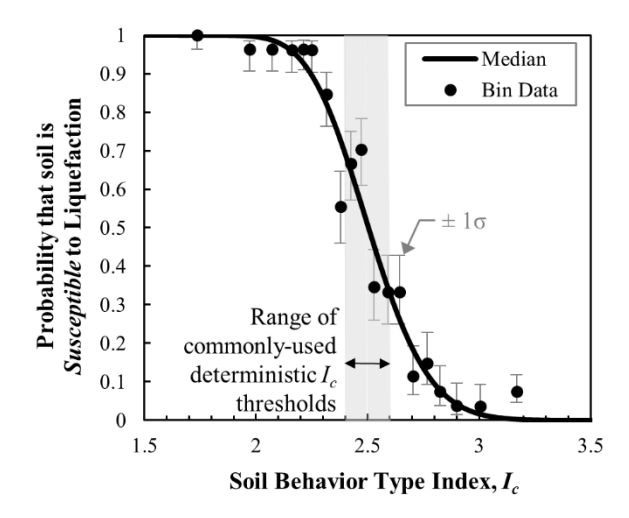


Figure 8. The probability of liquefaction susceptibility per the Boulanger and Idriss (2006) criterion as a function of measured I_c . The range of deterministic I_c thresholds commonly used in practice is also highlighted (Maurer et al., 2019).

Fines Content. Some liquefaction models use fines content (FC) as a predictive variable. As with liquefaction susceptibility, FC is best measured directly, but continuous sampling and measurement is not feasible for a large CPT campaign. Accordingly, CPT correlations developed from global data are commonly used to estimate FC but can often be improved via regional calibration. Analysts testing or training response models may thus be interested in the regional I_C

381

387

388

390

391

392

393

395

396

397

-FC correlations of Lees et al. (2015a) and Maurer et al. (2019). Lees et al. (2015a) calibrated the

general $I_c - FC$ correlation of Boulanger and Idriss (2014), wherein FC (%) is estimated as:

$$FC = 80 (I_c + C_{FC}) - 137 (9)$$

where C_{FC} is a calibration parameter that may adjust the general correlation (i.e., C_{FC} = 0) to regionspecific conditions. Analyzing 2,600 FC measurements from Canterbury, Lees et al. (2015a) proposed that C_{FC} = 0.2 was optimal. Using a similar amount of data but different processing and regression methods, Maurer et al. (2019) proposed that FC be estimated as:

$$\mu_{FC} = 80.645 I_c - 128.5967 \tag{10}$$

where μ_{FC} is the mean estimate of FC (%), limited to $0\% \le FC$ (%) $\le 100\%$. Guidance on using this correlation probabilistically is given in Maurer et al. (2019). A comparison of the Maurer et al. (2019) correlation and others, along with data from Christchurch, is shown in Figure 9.

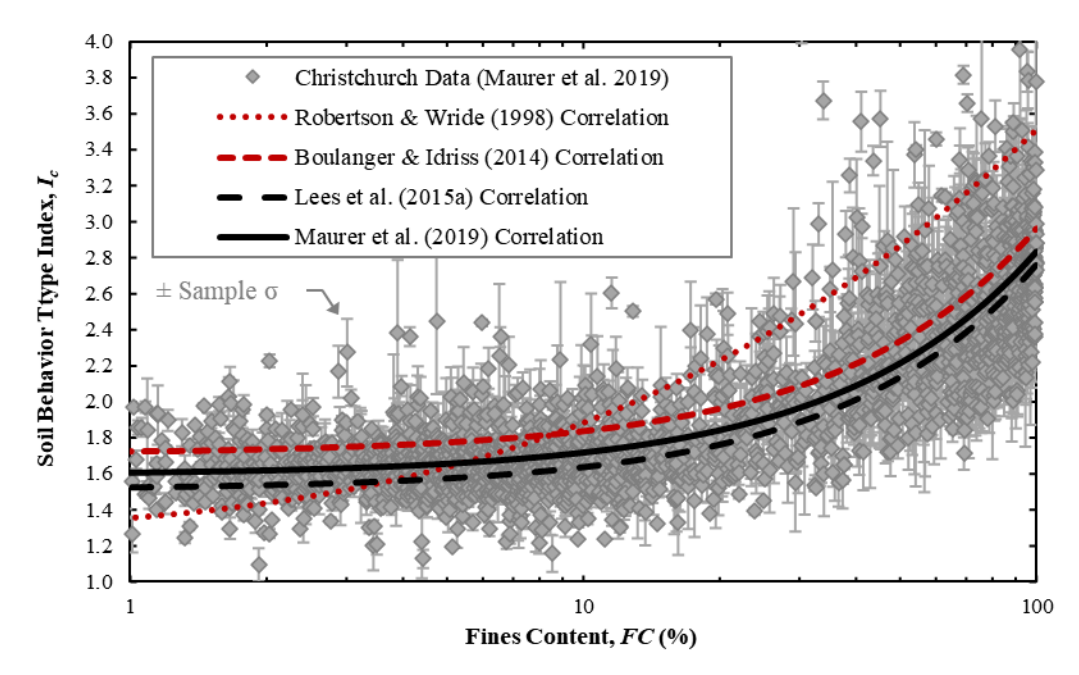


Figure 9. Canterbury $I_c - FC$ data and correlations (Lees et al. 2015a; Maurer et al. 2019), and comparison with the generic Robertson and Wride (1998) and Boulanger and Idriss (2014) correlations.

Soil Density. Total and effective vertical stresses are integral to CPT data processing and a common input to liquefaction models. While the authors are unaware of calibrated, Canterbury-specific correlations for estimating soil unit weights, several global correlations are available, including Mayne et al. (2010) and Robertson and Cabal (2010), with the latter being used in previous Canterbury earthquake research by the authors (e.g., Green et al. 2018; Geyin and Maurer 2019). While liquefaction models may be relatively insensitive to the adopted correlation, users should consider constraints, as needed and reasonable, to limit physically indefensible values.

GWT at Time of Testing. As discussed, the database contains event specific GWT depths, which are an estimate of conditions immediately prior to each earthquake. These may be used to infer the depth of saturation for assessing liquefaction susceptibility (to be further discussed) but may differ from the GWT depths at the time of testing, which are needed for CPT stress-normalization as part of routine data processing. While regional hydrologic models are unavailable for CPT test dates, which are shown in Figure 10a, most CPTs (\sim 90%) were performed between 22 Feb 2011 and 30 Sept 2013. In addition, it can be seen in Figures 10b and 10c that GWT depths in Feb 2011 were typically \sim 1% shallower relative to Sept 2010 and \sim 14% deeper relative to Feb 2016. In the absence of more rigorous modeling, adopting a GWT depth either interpolated from the three

estimates available, or simply averaged from the Feb 2011 and Feb 2016 values (since most CPTs were performed during this time), may provide a reasonable estimate for CPT stress normalization. Estimates could also be obtained from analyses of the CPT u2 data, although the reliability of this data due to issues with porous stone saturation, etc. is unknown for the compiled database.

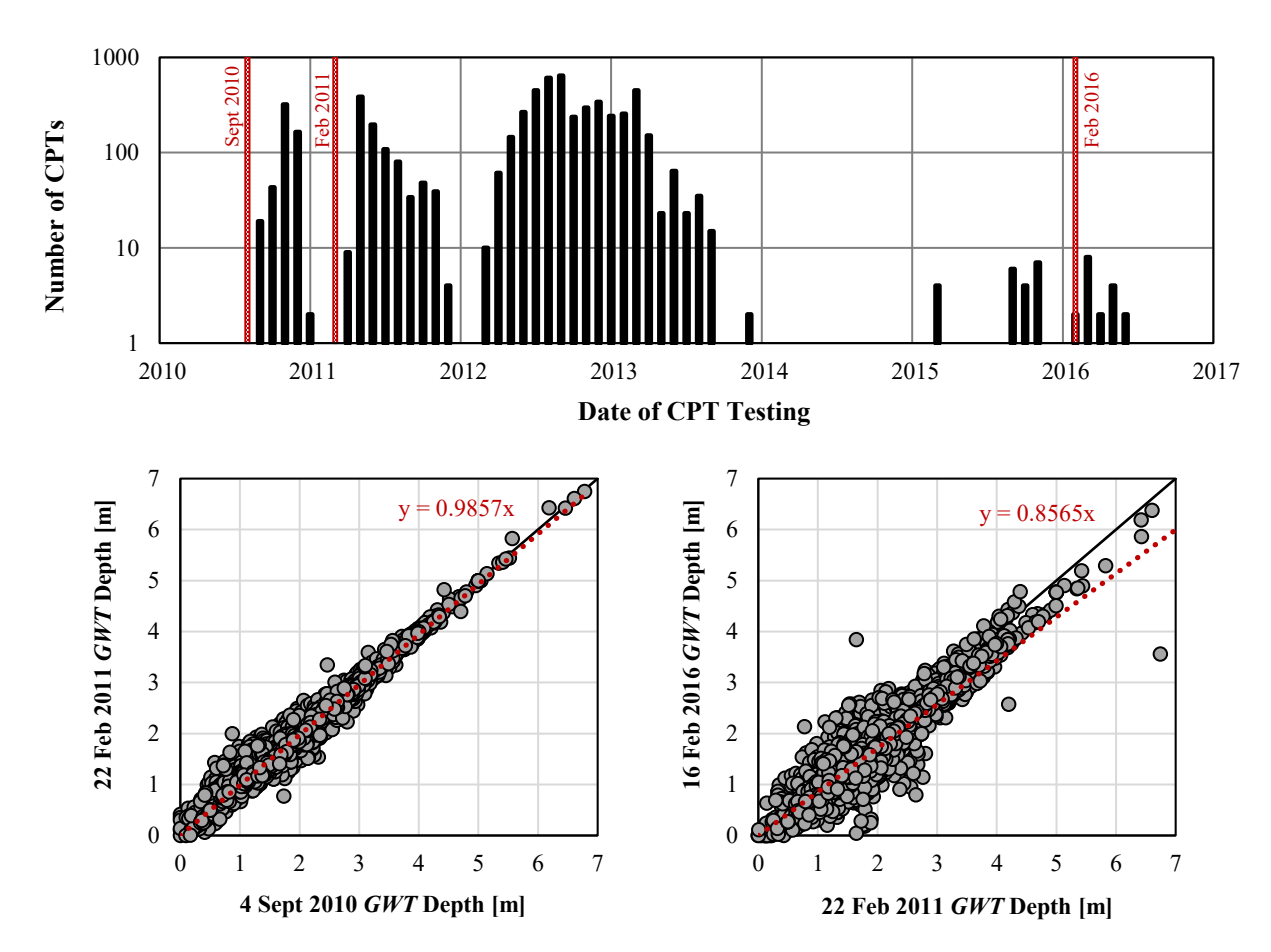


Figure 10. Case-history database statistics: **(a)** Monthly histogram of CPT test dates; **(b)** *GWT* depths from Sept 2010 versus Feb 2011; **(c)** *GWT* depths from Feb 2011 versus Feb 2016.

Model Training, Testing, and Bias. Historically, publications proposing, calibrating, or evaluating liquefaction models often lack standard test metrics (e.g., Maurer et al. 2015d), hindering quantifications and comparisons of model performance. Receiver-operating-characteristic (ROC) analyses (e.g., Fawcett 2006) are ubiquitous in medical diagnostics and data science (Zou 2007), and increasingly, are being adopted in geotechnical modelling (e.g., Oommen et al. 2010; Zhu et al. 2017; Green et al. 2017; Upadhyaya et al. 2020). ROC analyses provide a standard and objective assessment of prediction efficiency via the area-under-the-ROC-curve (AUC) and are relatively

insensitive to sampling imbalance (i.e., unequal positives and negatives). Analysts using the curated data to test or train liquefaction models should similarly adopt standard, objective, and repeatable measures of performance, be it ROC analyses or some other. In addition, while the Canterbury earthquakes resulted in a wealth of data, this data nonetheless samples the geologic and seismologic setting of one region, the findings from which may or may not translate elsewhere. Analysts should carefully consider sampling bias and weigh results from Canterbury with those from global case-histories (e.g., Brandenberg et al. 2020). Given that the compiled Canterbury database is much larger than that resulting from all other earthquakes combined, the finite-sample uncertainty of model performance should be computed for each respective database (e.g., via bootstrap sampling) and used to test for statistical significance. That is, to illustrate the sensitivity of performance to the data available for analysis, and to assess whether differences could arise from chance (i.e., due to finite sampling) and not because one model is better than another. As an example, p-values specific to ROC analyses may be computed per DeLong et al. (1988), an application of which is presented in Geyin et al. (2020a) for liquefaction case-history data.

Lingering Uncertainties

GWT Depth and Saturation. It is established that liquefaction resistance and degree of saturation are inversely related, all else being equal (e.g., Ishihara and Tsukamoto 2004; Hossain et al. 2013), and that soil beneath the apparent GWT can conceivably be less than 100% saturated (e.g., due to seasonal or tidal fluctuations, or to biologic activity). This phenomenon has been inferred from crosshole p-wave velocities (Cox et al. 2018) at select locations in Christchurch and investigated as a possible cause of observed mispredictions of liquefaction by popular models (McLaughlin 2017; Boulanger et al. 2018; Yost et al. 2019; Ntritsos and Cubrinovski, 2020). One detailed study of this issue is that of McLaughlin (2017), who analyzed 31 cases in Christchurch and computed liquefaction potential index (LPI) values with and without various corrections. These included corrections for partial saturation, site-specific FC, and inverse filtering and interface correction. While evidence of partial saturation was found at some locations, the corrections to LPI were typically minor compared to those made for FC and inverse filtering. The results of McLaughlin (2017) indicate that partial saturation beneath the GWT could potentially be important at some sites, but in general, does not sufficiently or consistently explain mispredictions of liquefaction. Nonetheless, uncertainties pertaining to partial saturation persist, but could only be adequately

addressed via extensive additional in-situ testing and/or regional hydrologic modeling. Owing to the rarity of p-wave measurements in parallel with CPTs, it is unknown whether partial saturation beneath the *GWT* is present in other case-histories, previously collected elsewhere globally.

CPT Spacing in Time. As discussed, multiple case-histories were often developed from a single site (i.e., CPT) affected by multiple earthquakes, wherein the event-specific GWT, PGA, and response were known. This raises the question of whether a CPT performed at one moment in time (predominantly between Feb 2011 and Sept 2013; see Figure 10a) is representative of a soil profile at multiple other times when earthquakes occurred? This will be addressed in three parts.

First, does the approach taken break from precedent? When considering all liquefaction case histories published to-date (e.g., Boulanger and Idriss 2014), in-situ testing has been performed: (i) well in advance of an earthquake; (ii) months-to-years after an earthquake; (iii) decades after an earthquake; and (iv) all scenarios in between. Additionally, between the time of in-situ testing and the occurrence of an earthquake, or between the time of the occurrence of an earthquake and in-situ testing, it is often the case that multiple other earthquakes of varying intensity have affected a site. In the authors' opinion, there has historically been no standard, or best practice, for the relative timing of in-situ testing when publishing liquefaction case-histories. The Boulanger and Idriss (2014) global database contains cases representing each of the four scenarios above, with multiple case histories based on the same CPT. Of the 255 case histories compiled therein, 25% are cases in which one CPT was used to develop multiple case histories. As an example, four case histories were developed from one CPT effected by earthquakes occurring over a 10-year span.

Second, does CPT data change over time once deposited or disturbed? Increases in the strength and stiffness of sands over time, or "aging effects," have been widely investigated. Temporal gains have been discerned both from penetration resistance, with reported gains of 3-7% per log-cycle in years (Mesri et al. 1990; Kulhawy and Mayne 1990), and from liquefaction resistance (i.e., CRR), with reported gains of 9-17% per log-cycle in years (Arango et al. 2000; Hayati and Andrus 2009; Saftner et al. 2015). It has thus been proposed that aging effects may be resolved into gains measurable by intermediate-to-large-strain penetration data and gains in liquefaction resistance, where the latter is influenced by small-strain fabric phenomena difficult to detect at large strain (Leon et al. 2006). Of relevance to the compilation of case histories, CPT measurements could conceivably vary with time, particularly over short time scales following liquefaction. For example, assuming the rates above, and that a soil is "reset" following

liquefaction, CPT resistance measured 1 month after an earthquake could be 3-7% less than if measured 1 year later. While such changes are plausible, they would be difficult to distinguish from site variability and measurement uncertainty, and to-date, have not been considered in casehistory publications.

488

489

490

491

492

493

494

495

496

497

498

499

500

501

502

503

504

505

506

507

508

509

510

511

512

513

514

515

516

Third, does CPT data change due to repeated disturbance from shaking, and if so, does the magnitude and direction of change (e.g., an increase or decrease in penetration resistance) depend on whether liquefaction did or did not occur? A closely related, but different question, is whether liquefaction resistance changes due to prior shaking/liquefaction, even if CPT data does not change? Researchers have sought answers to these questions using a variety of approaches: (i) CPT testing in the field before and after shaking/liquefaction (e.g., Lees et al. 2015b; Finno et al. 2016); (ii) CPT testing in centrifuge and shaking-table models, before and after shaking/liquefaction (e.g. Darby et al. 2016; Dobry et al. 2019); and (iii) cyclic triaxial and cyclic simple-shear tests wherein samples were subjected to multiple shaking/liquefaction sequences (e.g., Ha et al. 2011; Wang et al. 2013). Various conclusions were collectively drawn from these experiments, including: (i) penetration resistance increases; (ii) penetration resistance decreases; (iii) penetration resistance does not change, even after severe liquefaction; (iv) penetration resistance changes in some parts of the profile but not others; (v) the magnitude and direction of the change in penetration resistance depends on the number of previous shaking cycles, and on the pore pressure generated by those cycles; and (vi) liquefaction resistance may change, independent of whether this change is detected via CPT data. Most relevant to the current effort, perhaps, is the work of Lees et al. (2015b), who studied pairs of CPTs performed at 30 locations before and after the 22 Feb 2011 Christchurch earthquake, concluding that CPT measurements did not change in a statistically significant manner.

In summary, the approach taken by this study is consistent with past precedent. Additionally, questions pertaining to CPT data and soil response during earthquake sequences – which are very worthy of investigation – have not been adequately resolved to suggest when CPTs should or should not be used to compile liquefaction case histories. However, the compiled dataset could potentially be analyzed to further study these issues in the field, making use of the provided CPT coordinates and test dates.

Conclusions

517

518

519

520

521

522

523

524

525

526

527

528

535

Earthquakes occurring over the last decade in Canterbury, New Zealand, resulted in liquefaction case-history data of unprecedented quantity. Accordingly, this paper presented a curated dataset containing ~15,000 CPT-based liquefaction case-histories compiled from three earthquakes in this sequence. The compiled, post-processed data was provided in a dense array structure, allowing researchers to easily access and analyze information pertinent to CPT-based site characterization and free-field liquefaction response. Research opportunities using this data include, but are not limited to, the training or testing of new and existing liquefaction-prediction models. The many methods used to obtain and process the case-history data were detailed herein, as was the structure of the compiled file. Numerous recommendations for analyzing the data were also outlined, including nuances and limitations that users should carefully consider prior to analysis.

Acknowledgements

- The authors gratefully acknowledge Jason Motha of the University of Canterbury, New Zealand,
- for converting the case-history dataset into a python-compatible data frame.

531 **Data Availability**

- The Canterbury dataset is available in digital format through the NEHRI DesignSafe Data Depot
- at https://doi.org/10.17603/ds2-tygh-ht91. Additionally, Appendices A and B are provided as an
- electronic supplement to this paper.

Funding

- 536 The presented study is based on work supported by the National Science Foundation (NSF), US
- Geological Survey (USGS), and Pacific Earthquake Engineering Research Center (PEER) under
- 538 Grants CMMI-1751216, CMMI-1825189, CMMI-1937984, G18AP-00006, and 1132-NCTRBM,
- respectively. This work was also partially supported by QuakeCoRE, the New Zealand Centre for
- Earthquake Resilience, and is QuakeCoRE publication 0616. The authors also acknowledge the
- countless people who contributed to the liquefaction case-history data studied herein, which was
- 542 collected under the auspices the New Zealand Earthquake Commission (EQC). However, any
- opinions, findings, and conclusions or recommendations expressed in this paper are those of the
- authors and do not necessarily reflect the views of NSF, USGS, PEER, QuakeCoRE, or EQC.

545 REFERENCES

- 546 Abrahamson NA and Youngs, RR (1992) A stable algorithm for regression analyses using the random
- effects model. *Bulletin of the Seismological Society of America* 82(1): 505–510.
- 548 Ahmadi MM and Robertson PK (2005) Thin-layer effects on the CPT qc measurement. Canadian
- 549 *Geotechnical Journal* 42(5): 1302-1317.
- Anselin L (1995) Local indicators of spatial association—LISA. *Geographical analysis* 27(2): 93-115.
- Arango I, Lewis MR and Kramer C. (2000) Updated liquefaction potential analysis eliminates foundation
- retrofitting of two critical structures. *Soil Dynamics and Earthquake Engineering* 20: 17-25.
- Begg J and Jones K (2012) 20,000 years of time in Christchurch. Presentation to New Zealand Geotechnical
- 554 Society, Canterbury Branch, June 28, 2012, New Zealand Geotechnical Society, Wellington, New
- Zealand.
- Boulanger RW and DeJong JT (2018) Inverse filtering procedure to correct cone penetration data for thin-
- layer and transition effects. Cone Penetration Testing 2018, Hicks, Pisano, and Peuchen, eds., Delft
- University of Technology, The Netherlands: 25-44.
- Boulanger RW and Idriss IM (2006) Liquefaction susceptibility criteria for silts and clays. Journal of
- *Geotechnical and Geoenvironmental Engineering* 132(11): 1413-1426.
- Boulanger RW and Idriss IM (2007) Evaluation of cyclic softening in silts and clays. Journal of
- *Geotechnical and Geoenvironmental Engineering* 133(6): 641–652.
- Boulanger RW and Idriss IM (2014) CPT and SPT Based Liquefaction Triggering Procedures, Report No.
- 564 *UCD/CGM-14/01*, Center for Geotechnical Modeling, University of California, Davis, CA.
- Boulanger RW, Khosravi M, Cox BR and DeJong JT (2019) Liquefaction Evaluation for an Interbedded
- Soil Deposit: St. Teresa's School, Christchurch, New Zealand. IACGE 2018: Geotechnical and Seismic
- *Research and Practices for Sustainability*: 686-704.
- Bradley BA (2012) Strong ground motion characteristics observed in the 4 September 2010 Darfield, New
- Zealand earthquake. *Soil Dynamics and Earthquake Engineering* 42: 32–46.
- 570 Bradley BA (2013) A New Zealand-specific pseudo spectral acceleration ground-motion prediction
- equation for active shallow crustal earthquakes based on foreign models. Bulletin of the Seismological
- *Society of America* 103(3):1801–1822.
- 573 Bradley BA (2014) Site-specific and spatially-distributed ground motion intensity estimation in the 2010-
- 574 2011 Christchurch earthquakes. *Soil Dynamics and Earthquake Engineering* 48: 35-47.
- 575 Bradley BA (2016) Strong ground motion characteristics observed in the 13 June 2011 Mw6.0
- 576 Christchurch, New Zealand earthquake. *Soil Dynamics and Earthquake Engineering* 91: 23-38.
- 577 Bradley BA and Cubrinovski M (2011) Near-source strong ground motions observed in the 22 February
- 578 2011 Christchurch earthquake. Seismological Research Letters 82(6): 853–865.

- 579 Bradley BA, and Hughes, M (2012) Conditional peak ground accelerations in the Canterbury earthquakes
- for conventional liquefaction assessment. *University of Canterbury, Christchurch, New Zealand*.
- Bradley BA, Savarimuthu S, Lagrava D, Huang J, Motha J, Polak V and Bae S (2017) SeisFinder: A web
- application for extraction of data from computationally-intensive earthquake resilience calculations.
- Poster Presentation at 2017 SCEC Annual Meeting. Palm Springs, CA.
- Brandenberg SJ, Zimmaro P, Stewart JP, Kwak DY, Franke KW, Moss RE, ... Kramer SL. (2020) Next-
- generation liquefaction database. *Earthquake Spectra*, Doi: 10.1177/8755293020902477.
- Bray JD and Sancio RB (2006) Assessment of the liquefaction susceptibility of fine-grained soils. *Journal*
- of Geotechnical and Geoenvironmental Engineering 132(9): 1165-1177.
- Bray J, Cubrinovski M, Zupan J, and Taylor M (2014) Liquefaction effects on buildings in the central
- business district of Christchurch. *Earthquake Spectra* 30(1): 85–109.
- Brown LJ (1975) Water well data. Sheet 576/7-8, Belfast-Styx. New Zealand Geological Survey, Report
- 591 72.
- Brown LJ and Weeber JH (1992) Geology of the Christchurch urban area: Institute of Geological and
- Nuclear Sciences Geological Map 1. Institute of Geological and Nuclear Sciences Limited, Lower Hutt,
- *New Zealand, scale, 1*(25,000), 1.
- Brown LJ, Beetham RD, Paterson BR and Weeber JH (1995) Geology of Christchurch, New Zealand.
- *Environmental Engineering and Geoscience* 1(4): 427–488.
- 597 Buck JR, Daniel MM and Singer AC (2002) Computer Explorations in Signals and Systems Using
- 598 *MATLAB*®, 2nd Edition. Upper Saddle River, NJ: Prentice Hall.
- 599 CERA (2013) Purpose and scope of the Canterbury geotechnical database. Canterbury Earthquake
- Recovery Authority, Information Note, Revision D. Christchurch, New Zealand.
- 601 Chalmers G, McLennan N and Barsanti L (2013) Lyttelton port of Christchurch seismic resilience from an
- owners' perspective. Proceedings of Ports 2013: Success Through Diversification: 1405-1414.
- 603 Cox BR, Stolte AC, Stokoe KH and Wotherspoon LM. (2018) A Direct-Push Crosshole (DPCH) Test
- Method for the In Situ Evaluation of High-Resolution P-and S-Wave Velocities. *Geotechnical Testing*
- 605 *Journal* 42(5): 1101-1132.
- 606 Cubrinovski M, Bray JD, Taylor M, Giorgini S, Bradley BA, Wotherspoon L and Zupan J (2011) Soil
- liquefaction effects in the central business district during the February 2011 Christchurch earthquake.
- 608 Seismological Research Letters 82: 893–904.
- 609 Cubrinovski M, Winkley A, Haskell J, Palermo A, Wotherspoon L, Robinson K, Bradley B, Brabhaharan
- P and Hughes, M (2014) Spreading-induced damage to short-span bridges in Christchurch, New
- Zealand. Earthquake Spectra 30(1): 57–83.

- 612 Cubrinovski, M, and Robinson, K, (2016) Lateral spreading: Evidence and interpretation from the 2010-
- 613 2011 Christchurch earthquakes. *Soil Dynamics and Earthquake Engineering* 91: 187-201.
- Darby KM, Bronner JD, Parra Bastidas AM, Boulanger RW and DeJong JT (2016) Effect of shaking history
- on the cone penetration resistance and cyclic strength of saturated sand. In Geotechnical and Structural
- 616 Engineering Congress 2016: 1460-1471.
- DeLong ER, DeLong DM and Clarke-Pearson DL (1988) Comparing the areas under two or more
- correlated receiver operating characteristic curves: a nonparametric approach. *Biometrics* 44: 837-845.
- de Magistris, FS, Lanzano G, Forte G, and Fabbrocino, G (2013) A database for PGA threshold in
- 620 liquefaction occurrence. Soil Dynamics and Earthquake Engineering 54: 17-19.
- Dobry R, Ladd RS, Yokel FY, Chung RM and Powell D (1982) Prediction of pore water pressure buildup
- and liquefaction of sands during earthquakes by the cyclic strain method (Vol. 138). Gaithersburg, MD:
- National Bureau of Standards.
- Dobry R, Thevanayagam S, El-Sekelly W, Abdoun T and Huang Q (2019) Large-Scale Modeling of
- Preshaking Effect on Liquefaction Resistance, Shear Wave Velocity, and CPT Tip Resistance of Clean
- Sand. Journal of Geotechnical and Geoenvironmental Engineering 145(10): 04019065.
- Fawcett T (2006) An introduction to ROC analysis. Pattern Recognition Letters 27(8): 861–874.
- 628 Finno RJ, Gallant AP and Sabatini PJ (2016) Evaluating ground improvement after blast densification:
- 629 performance at the Oakridge landfill. Journal of Geotechnical and Geoenvironmental
- 630 Engineering 142(1): 04015054.
- 631 Geyin M and Maurer BW (2019) An analysis of liquefaction-induced free-field ground settlement using
- 632 1,000+ case-histories: observations vs. state-of-practice predictions. Geocongress 2019: Earthquake
- Engineering and Soil Dynamics (C.L. Meehan, S. Kumar, M.A. Pando, and J.T. Coe, eds.), Geotechnical
- 634 Special Publication 308: 489-498.
- 635 Geyin M, Baird AJ and Maurer BW (2020a) Field assessment of liquefaction prediction models based on
- geotechnical vs. geospatial data, with lessons for each. Earthquake Spectra 36(3): 1386–1411.
- 637 Geyin, M., Maurer, B.W., Bradley, B.A., Green, R.A., and van Ballegooy, S. (2020b). "CPT-Based
- 638 Liquefaction Case Histories Resulting from the 2010-2016 Canterbury, New Zealand, Earthquakes: A
- Curated Digital Dataset (Version 2)." DesignSafe-CI. https://doi.org/10.17603/ds2-tygh-ht91.
- 640 Geyin M and Maurer BW (2020a) Horizon: CPT-based liquefaction risk assessment and decision software.
- DesignSafe-CI, doi: 10.17603/ds2-2fky-tm46.
- 642 Geyin M and Maurer BW (2020b) Fragility functions for liquefaction induced ground failure. *Journal of*
- Geotechnical and Geoenvironmental Engineering, doi: 10.1061/(ASCE)GT.1943-5606.0002416.
- Goda K and Hong HP (2008) Spatial correlation of peak ground motions and response spectra. Bulletin of
- the Seismological Society of America 98(1): 354–365.

- 646 Green RA, Allen A, Wotherspoon L, Cubrinovski M, Bradley B, Bradshaw A, Cox B and Algie T (2011)
- Performance of levees (stopbanks) during the 4 September M_w7.1 Darfield and 22 February 2011 M_w6.2
- Christchurch, New Zealand, earthquakes. Seismological Research Letters 82(6): 939–949.
- 649 Green RA, Cubrinovski M, Cox B, Wood C, Wotherspoon L, Bradley B and Maurer B (2014) Select
- Liquefaction Case Histories from the 2010-2011 Canterbury Earthquake Sequence. Earthquake Spectra
- 651 30(1): 131-153.
- 652 Green RA and Ziotopoulou K (2015). Overview of screening criteria for liquefaction triggering
- susceptibility. *Proceedings of the 10th Pacific Conference on Earthquake Engineering*, Nov 6-8, Sydney,
- Australia. Australian Earthquake Engineering Society; Paper No. 35. 2015.
- 655 Green RA, Upadhyaya S, Wood C, Maurer BW, Cox BR, Wotherspoon L, Bradley BA and Cubrinovski M
- 656 (2017) Relative efficacy of CPT- versus Vs based simplified liquefaction evaluation procedures. 19th
- International Conference on Soil Mechanics and Geotechnical Engineering, 1521-1524.
- 658 Green RA, Maurer BW and van Ballegooy S (2018) The influence of the non-liquefied crust on the severity
- of surficial liquefaction manifestations: case history from the 2016 Valentine's Day earthquake in New
- Zealand. Geotechnical Earthquake Engineering and Soil Dynamics V: Liquefaction Triggering,
- Consequences, and Mitigation (S.J. Brandenberg and M.T. Manzari, eds.), Geotechnical Special
- 662 Publication 290: 21-32.
- 663 Green RA, Bommer JJ, Rodriguez-Marek A, Maurer BW, Stafford PJ, Edwards B, Kruiver PP, De Lange G
- and Van Elk J (2019) Addressing limitations in existing 'simplified' liquefaction triggering evaluation
- procedures: application to induced seismicity in the Groningen gas field. Bulletin of Earthquake
- 666 Engineering 17(8): 4539-4557.
- Ha IS, Olson SM, Seo MW and Kim MM (2011) Evaluation of reliquefaction resistance using shaking table
- tests. Soil dynamics and earthquake engineering 31(4): 682-691.
- Hayati H and Andrus RD (2009) Updated liquefaction resistance correction factors for aged sands. Journal
- of geotechnical and geoenvironmental engineering 135(11): 1683-1692.
- Hossain AM, Andrus RD and Camp III WM (2013) Correcting liquefaction resistance of unsaturated soil
- using wave velocity. *Journal of Geotechnical and Geoenvironmental Engineering* 139(2): 277-287.
- 673 Ishihara K and Tsukamoto Y (2004) Cyclic strength of imperfectly saturated sands and analysis of
- 674 liquefaction. *Proceedings of the Japan Academy, Series B*, 80(8): 372-391.
- Jeffries MG and Davies MP (1993) Use of CPTu to estimate equivalent SPTN60. Geotechnical Testing
- 676 *Journal* 16(4): 458–468.
- Johnson RA and Wichern DW (2007) Applied multivariate statistical analysis, Pearson Prentice Hall, Upper
- 678 Saddle River, NJ.

- Kramer SL, Sideras SS and Greenfield MW (2016) The timing of liquefaction and its utility in liquefaction
- hazard evaluation. Soil Dynamics and Earthquake Engineering 91: 133-146.
- Kulhawy FH and Mayne PW (1990) Manual on estimating soil properties for foundation design. Final Rep.
- 682 1493-6, EL-6800, Electric Power Research Institute, Palo Alto, Calif
- 683 Kwasinski A, Eidinger J, Tang A, and Tudo-Bornarel C (2014) Performance of electric power systems in
- the 2010–2011 Christchurch, New Zealand, earthquake sequence. *Earthquake Spectra* 30(1): 205–230.
- Lees J, van Ballegooy S and Wentz FJ (2015a) Liquefaction susceptibility and fines content correlations of
- the Christchurch soils. Proceedings of the 6th international conference on earthquake geotechnical
- 687 engineering. Nov 2-4; Christchurch, New Zealand; Paper No. 491.
- Lees J, Ballagh RH, Orense RP and Van Ballegooy S (2015b) CPT-based analysis of liquefaction and re-
- 689 liquefaction following the Canterbury earthquake sequence. Soil Dynamics and Earthquake
- 690 Engineering 79: 304-314.
- Leon E, Gassman SL and Talwani P (2006) Accounting for soil aging when assessing liquefaction potential.
- *Journal of Geotechnical and Geoenvironmental Engineering* 132(3): 363-377.
- 693 Li DK, Juang CH, Andrus, RD and Camp WM (2007) Index properties-based criteria for liquefaction
- susceptibility of clayey soils: a critical assessment. Journal of Geotechnical and Geoenvironmental
- 695 Engineering 133(1): 110-115.
- 696 Lunne T, Robertson PK and Powell JM (1997) Cone Penetration Testing in Geotechnical Practice. Blackie
- 697 Academic & Professional, London, U.K.
- Mayne PW, Peuchen J and Bouwmeester D (2010) Soil unit weight estimation from CPTs. 2nd
- 699 International symposium on cone penetration testing, 8p
- McLaughlin K (2017) Investigation of false-positive liquefaction case history sites in Christchurch, New
- Zealand. M.S. Thesis. The University of Texas at Austin, Austin, TX.
- Maurer BW, Green RA, Cubrinovski M and Bradley BA (2014) Evaluation of the liquefaction potential
- index for assessing liquefaction hazard in Christchurch, New Zealand. Journal of Geotechnical and
- Geoenvironmental Engineering 140(7): 04014032.
- Maurer BW, Green RA, Cubrinovski M and Bradley BA (2015a) Fines-content effects on liquefaction
- hazard evaluation for infrastructure during the 2010-2011 Canterbury, New Zealand earthquake
- sequence. Soil Dynamics and Earthquake Engineering 76: 58-68.
- 708 Maurer BW, Green RA and Taylor ODS (2015b) Moving towards an improved index for assessing
- 709 liquefaction hazard: lessons from historical data. *Soils and Foundations* 55(4): 778-787.
- 710 Maurer BW, Green RA, Cubrinovski M and Bradley B (2015c) Assessment of CPT-based methods for
- 711 liquefaction evaluation in a liquefaction potential index framework. *Géotechnique* 65(5): 328-336.

- Maurer BW, Green RA, Cubrinovski M and Bradley BA (2015d) Calibrating the liquefaction severity
- number (LSN) for varying misprediction economies: a case study in Christchurch, New Zealand. 6th
- 714 International Conference on Earthquake Geotechnical Engineering, Paper No. 491.
- 715 Maurer BW, Green RA, van Ballegooy S and Wotherspoon L (2019) Development of region-specific soil
- behavior type index correlations for evaluating liquefaction hazard in Christchurch, New Zealand. Soil
- 717 *Dynamics and Earthquake Engineering* 117: 96-105.
- 718 Mesri G, Feng T and Benak JM (1990) Postdensification penetration resistance of clean sands. *Journal of*
- 719 *Geotechnical Engineering* 116(7): 1095–1115.
- 720 Moss RES, Seed RB, Kayen RE, Stewart JP, Der Kiureghian A and Cetin KO (2006) CPT-based
- probabilistic and deterministic assessment of in situ seismic soil liquefaction potential. *Journal of*
- Geotechnical and Geoenvironmental Engineering 132(8): 1032-1051.
- National Research Council (NRC) (2016) State of the Art and Practice in the Assessment of Earthquake
- 724 Induced Soil Liquefaction and its Consequences, Committee on Earthquake Induced Soil Liquefaction
- Assessment (Edward Kavazanjian, Jr., Chair, Jose E. Andrade, Kandian "Arul" Arulmoli, Brian F.
- Atwater, John T. Christian, Russell A. Green, Steven L. Kramer, Lelio Mejia, James K. Mitchell, Ellen
- Rathje, James R. Rice, and Yumie Wang), The National Academies Press, Washington, DC.
- 728 Ntritsos N and Cubrinovski M (2020) A CPT based effective stress analysis procedure for liquefaction
- assessment. Soil Dynamics and Earthquake Engineering 131: 106063.
- 730 NZGD (2020) New Zealand Geotechnical Database. New Zealand Earthquake Commission.
- 731 https://www.nzgd.org.nz/, (Accessed Jan 01, 2020).
- O'Rourke T, Jeon SS, Toprak S, Cubrinovski M, Hughes M, van Ballegooy S and Bouziou D (2014)
- Earthquake response of underground pipeline networks in Christchurch, NZ. *Earthquake Spectra* 30(1):
- 734 183–204.
- Pease JW (2010) Misclassification in CPT liquefaction evaluation. 2nd International Symposium on Cone
- 736 *Penetration Testing.* Huntington Beach, CA, Paper # 3-23. 2010.
- Pinheiro J, Bates DM, DebRoy S, Sarkar D and the R Core Team. (2008). NLME: Linear and nonlinear
- mixed effects models, R Corepackage, Ver. 3.1, http://www.r-project.org (Mar. 26, 2014).
- Polito C (2001) Plasticity Based Liquefaction Criteria. Proceedings of the Fourth International Conference
- on Recent Advances in Geotechnical Earthquake Engineering and Soil Dynamics, San Diego,
- 741 California, March 26-31. Paper 25.
- 742 Quigley MC, Bastin S and Bradley BA (2013) Recurrent liquefaction in Christchurch, New Zealand, during
- the Canterbury earthquake sequence. *Geology* 41: 419–422.

- Quigley MC, Hughes MW, Bradley BA, van Ballegooy S, Reid C, Morgenroth J, Horton T, Duffy B, and
- Pettinga J (2016) The 2010-2011 Canterbury earthquake sequence: Environmental effects, seismic
- triggering thresholds, geologic legacy. *Tectonophysics* 672-673: 228-274.
- Rashidian V and Gillins DT (2018) Modification of the liquefaction potential index to consider the
- topography in Christchurch, New Zealand. *Engineering Geology* 232: 68-81.
- Robertson PK (2011) Automated detection of CPT transition zones. *Geotechnical News*, June: 35-38.
- Robertson PK and Wride CE (1998) Evaluating cyclic liquefaction potential using cone penetration test.
- 751 Canadian Geotechnical Journal 35(3): 442-459.
- Robertson PK and Cabal KL (2010) Estimating soil unit weight from CPT. 2nd Int. Symp. on Cone
- 753 Penetration Testing, 8p.
- 754 Saftner DA, Green RA and Hryciw RD (2015) Use of Explosives to Investigate Liquefaction Resistance of
- Aged Sand Deposits. *Engineering Geology* 199: 140-147.
- Seed RB, Cetin KO, Moss RES, Kammerer AM, Wu J, Pestana JM, Riemer MF, Sancio RB, Bray JD,
- Kayen RE and Faris A (2003) Recent advances in soil liquefaction engineering: a unified and consistent
- framework. 26th Annual ASCE Los Angeles Geotechnical Spring Seminar. 30 April, Long Beach, CA.
- 759 Seisfinder (2020). *A web application to enable the extraction of high-fidelity outputs from computationally*
- 760 intensive earthquake resilience calculations. Accessed 1 August 2020 https://quakecoresoft.
- 761 canterbury.ac.nz/seisfinder/>
- Sideras S (2019) Evolutionary Intensity Measures for More Accurate and Informative Evaluation of
- Liquefaction Triggering. PhD Dissertation, University of Washington, Seattle, WA.
- 764 Tang A, Kwasinski A, Eidinger J, Foster C, and Anderson P (2014) Telecommunication systems'
- performance: Christchurch earthquakes. *Earthquake Spectra* 30(1): 231–252.
- Townsend D, Lee JM, Strong DT, Jongens R, Smith Lyttle B, Ashraf S, ... and Taylor ML (2016) Mapping
- surface liquefaction caused by the September 2010 and February 2011 Canterbury earthquakes: A digital
- dataset. New Zealand Journal of Geology and Geophysics 59(4): 496-513.
- Treadwell DD (1976) The influence of gravity, prestress, compressibility, and layering on soil resistance to
- static penetration. PhD Dissertation, Univ. of California, Berkeley, CA.
- Upadhyaya S, Green RA, Rodriguez-Marek A, Maurer BW, Wotherspoon L, Bradley BA and Cubrinovski
- 772 M (2019) Influence of corrections to recorded peak ground accelerations due to liquefaction on predicted
- liquefaction response during the 2010-2011 Canterbury, New Zealand, earthquake sequence. In *Proc.*
- 13th Australia New Zealand Conference on Geomechanics (13ANZCG).
- 775 Upadhyaya S, Maurer BW, Green RA and Rodriguez-Marek A (2020) Selecting the Optimal Factor of
- Safety or Probability of Liquefaction Triggering for Engineering Projects Based on Misprediction Costs.
- Journal of Geotechnical and Geoenvironmental Engineering, (in review).

- van Ballegooy S, Malan P, Lacrosse V, Jacka ME, Cubrinovski M, Bray JD, O'Rourke TD, Crawford SA
- and Cowan H (2014a) Assessment of liquefaction-induced land damage for residential Christchurch.
- 780 *Earthquake Spectra* 30(1): 31-55.
- van Ballegooy S, Cox SC, Thurlow C, Rutter HK, Reynolds T, Harrington G, Fraser J and Smith T (2014b)
- Median water table elevation in Christchurch and surrounding area after the 4 September 2010 Darfield
- earthquake: Version 2. GNS Science Report 2014/18, 2014b.
- van Ballegooy S, Green RA, Lees J, Wentz F and Maurer BW (2015) Assessment of various CPT based
- 785 liquefaction severity index frameworks relative to the Ishihara (1985) H₁-H₂ boundary curves. Soil
- 786 Dynamics and Earthquake Engineering 79: 347-364.
- van der Linden TI, De Lange DA and Korff M (2018) Cone penetration testing in thinly inter-layered soils.
- 788 Proceedings of the Institution of Civil Engineers-Geotechnical Engineering 171(3): 215-231.
- Wang S, Yang J and Onyejekwe S (2013) Effect of previous cyclic shearing on liquefaction resistance of
- 790 Mississippi River Valley silt. *Journal of materials in civil engineering* 25(10): 1415-1423.
- Wotherspoon L, Bradshaw A, Green RA, Wood C, Palermo A, Cubrinovski M and Bradley BA (2011)
- Performance of bridges during the 2010 Darfield and 2011 Christchurch earthquakes. Seismological
- 793 Research Letters 82(6): 950–964.
- Wotherspoon LM, Orense RP, Green RA, Bradley BA, Cox BR and Wood CM (2015) Assessment of
- 795 liquefaction evaluation procedures and severity index frameworks at Christchurch strong motion
- stations. *Soil Dynamics and Earthquake Engineering* 79: 335-346.
- Yost KM, Cox BR, Wotherspoon L, Boulanger RW, van Ballegooy S and Cubrinovski M (2019) In Situ
- 798 Investigation of False-Positive Liquefaction Sites in Christchurch, New Zealand: Palinurus Road Case
- History. *Geo-Congress 2019: Earthquake Engineering and Soil Dynamics* 436-451.
- Yost KM, Green RA, Upadhyaya S, Maurer BW, Yerro-Colom A and Martin E (2020) Assessment of the
- 801 Efficacies of Correction Procedures for Multiple Thin Layer Effects on Cone Penetration Tests. Soil
- *Dynamics and Earthquake Engineering*, (in preparation).
- 803 Zhu J, Baise LG and Thompson EM (2017) An Updated Geospatial Liquefaction Model for Global
- Application. *Bulletin of the Seismological Society of America* 107(3): 1365-1385.
- 805 Zou KH (2007) Receiver operating characteristic (ROC) literature research. On-line bibliography,
- http://www.spl.harvard.edu/archive/spl-pre2007/pages/ppl/zou/roc.html